PERGAMON

Atmospheric Environment 35 (2001) 6073–6085

ATMOSPHERIC ENVIRONMENT

www.elsevier.com/locate/atmosenv

The effect of water on gas–particle partitioning of secondary organic aerosol: II. *m*-xylene and 1,3,5-trimethylbenzene photooxidation systems

David R. Cocker III, Brian T. Mader, Markus Kalberer, Richard C. Flagan, John H. Seinfeld*

Department of Environmental Engineering Science and Department of Chemical Engineering, California Institute of Technology, Pasadena, CA 91125, USA

Received 10 February 2001; accepted 29 July 2001

Abstract

An investigation of the effect of relative humidity on aerosol formation from *m*-xylene and 1,3,5-trimethylbenzene photooxidation is reported. Experiments were performed in the presence and absence of ammonium sulfate seed particles (both aqueous and dry) to ascertain the effect of partitioning of oxidation products into a strong electrolytic solution or onto dry crystalline seed particles. In marked contrast to the α-pinene/ozone system, the final measured secondary organic aerosol yield was unaffected by the presence of gas-phase or liquid-phase water at relative humidities (RH) up to 50%. The hygroscopic nature of the aerosol generated upon photooxidation of *m*-xylene and 1,3,5-trimethylbenzene was examined; the hygroscopicity of the aerosol at 85% RH for both parent organics increased with the extent of the reaction, indicating that the first-generation oxidation products undergo further oxidation. Limited identification of the gas- and aerosol-phase products of *m*-xylene and 1,3,5-trimethylbenzene photooxidation is reported. It is evident that a more complete molecular identification of aromatic photooxidation aerosol awaits analytical techniques not yet brought to bear on this problem.

1. Introduction

Aromatic hydrocarbons, a significant component of the gas-phase organic compounds in the urban atmosphere, form ozone and secondary organic aerosol (SOA) upon oxidation. For example, Odum et al. (1997a, b) determined that aerosols resulting from photooxidation of whole gasoline vapor could be attributed solely to the aromatic species in the gasoline. Until the recent work of Edney et al. (2000), the effect of relative humidity on the SOA yield from aromatic species had not been evaluated. Edney et al. (2000) estimated water uptake of the aerosol produced from toluene photooxidation using gravimetric analysis. Based on their results, they inferred that the presence of water does not affect SOA yield in the toluene system.

Part I reports an extensive investigation of the effect of relative humidity on the gas–particle partitioning of the oxidation products of the α-pinene/ozone reaction. In that system SOA yield is unaffected either in the presence or absence of a dry seed aerosol. After correction for aerosol water uptake, it was determined that gas-phase water does not affect the SOA yield whether or not dry seed particles are present. However, the presence of a strong aqueous electrolytic seed aerosol was found to decrease the SOA yield.

Identification of the aerosol molecular composition allows theoretical estimation of aerosol production, including the interaction with liquid water (Jang and Kamens, 1998; Ansari and Pandis, 2000). To date, only

*Corresponding author. Fax: +1-818-585-1729.
E-mail address: seinfeld@caltech.edu (J.H. Seinfeld).

1352-2310/01/$ - see front matter
PII: S1352-2310(01)00405-8

two studies have identified the molecular composition of aromatic oxidation products in conjunction with aerosol formation. Forstner et al. (1997) investigated seven aromatic compounds, toluene, *m*,*p*-xylene, *m*,*p*-ethyltoluene, ethylbenzene, and 1,2,4-trimethylbenzene. In these studies, aerosol products were collected on quartz filters, extracted, and then analyzed using GC–MS. Only 15–30% of the mass collected and extracted was identified. Several identified compounds measured on the filter were believed to be a result of vapor adsorption to the quartz filter rather than aerosol-phase constituents. Kleindienst et al. (1999) identified some gas-phase products of toluene, *p*-xylene, and 1,3,5-trimethylbenzene photooxidation in which aerosol was formed, but did not report specific molecular composition of the aerosol.

We report here the results of an investigation on the effect of relative humidity (RH) on SOA formation from *m*-xylene and 1,3,5-trimethylbenzene (1,3,5-TMB) photooxidation. First, we describe the experimental procedures used for these photooxidation experiments. Next, the hygroscopic nature of the oxidation products of *m*-xylene and 1,3,5-TMB is compared to that of α-pinene oxidation products. An evaluation of the SOA formation potential for *m*-xylene and 1,3,5-TMB for different experimental conditions follows. Finally, we report limited identification of the oxidation products of *m*-xylene and 1,3,5-TMB.

2. Experimental description

The chamber facility and basic experimental procedures and protocols are outlined in Part I. Those modifications and additions that are necessary specifically for photooxidation experiments are discussed below. Further detail of the chamber facility, protocols, and equipment used is found in Cocker et al., 2001.

The indoor chamber is illuminated using three-hundred 1.22 m GE350BL fluorescent blacklights. The integrated total light intensity is estimated by steady-state actinometry on NO_2. The photolysis rate of NO_2 in the current chamber configuration, is measured at $1.1\,min^{-1}$. The chambers were flushed with purified air for a minimum of 24 h prior to the start of an experiment. Three-hundred parts per billion propene (a photochemical initiator), NO, NO_2 and *m*-xylene or 1,3,5-TMB were introduced into the dark chamber. The total NO_x mixing ratio was set to a ppbC : ppb NO_x of 2 : 1. Hydrocarbon, NO_x, and ozone concentrations were measured prior to the start of the experiment. A minimum of three initial hydrocarbon measurements were taken for each chamber. Analysis were repeated every 11 min during the experiment. Ozone was monitored with a Dasibi Environmental Corp. (Glendale, CA) Model 1008-PC O_3 analyzer. NO and NO_2 were monitored with a Thermo Environmental Inc. (Woburn, MA) model 42 chemiluminescent NO–NO_2–NO_x analyzer. Ozone and NO_x measurements were taken during 10 min intervals, alternating between the two chambers. Temperature and relative humidity were monitored continuously.

3. Hygroscopic properties of *m*-xylene and 1,3,5-TMB aerosol oxidation products

The hygroscopic behavior of an aerosol is a measure of its physical response to variation in the relative humidity surrounding the particle. The hygroscopic growth factor (G_f), conventionally measured using a tandem differential mobility analyzer (TDMA) (McMurry and Stolzenburg, 1989), is defined as the ratio of the particle diameter at a given RH ($D_{p,h}$) to the dry particle diameter ($D_{p,d}$), $G_f = D_{p,h}/D_{p,d}$. In the current study, TDMA measurements were made on particles with dry diameters of 136 and 235 nm.

Growth factors for the nucleation products of *m*-xylene and 1,3,5-TMB photooxidation were obtained at 85% RH. Fig. 1a shows G_f as a function of the time of oxidation for both parent hydrocarbons. At the onset of the experiment, the G_f of the condensing organic aerosol is 1.0, indicating that the initial condensing species are hydrophobic. However, as the photooxidation progresses, the aerosol becomes more hygroscopic; G_f eventually reaches values of 1.12 and 1.10 for *m*-xylene and 1,3,5-TMB, respectively.

The increase of G_f (85% RH) over the course of the photooxidation strongly suggests that the initial hydrocarbon oxidation products undergo continued oxidation throughout the experiment, leading to products more hygroscopic than those initially formed. These hygroscopic products then partition to the aerosol-phase, increasing its affinity for water. Alternatively, aerosol-phase oxidation might lead to the more hydrophilic aerosol-phase products. In either event, the changing water affinity clearly shows that the aerosol composition evolves over time. Therefore, it is critical, when performing molecular composition studies, that the extent of the oxidation be considered. It is not surprising that more highly oxidized species are more hygroscopic since further oxidation will likely lead to multiple oxygenated functional groups. These are expected to be more polar and have higher water affinity.

The increase in the hygroscopicity of the *m*-xylene and 1,3,5-TMB aerosol at 85% RH over the course of oxidation contrasts with that observed for α-pinene ozonolysis. Fig. 1b shows G_f as a function of time of oxidation for α-pinene ozonolysis at 303 K. For α-pinene, the value of G_f early in the experiment is 1.065, indicating that the species that condense initially are

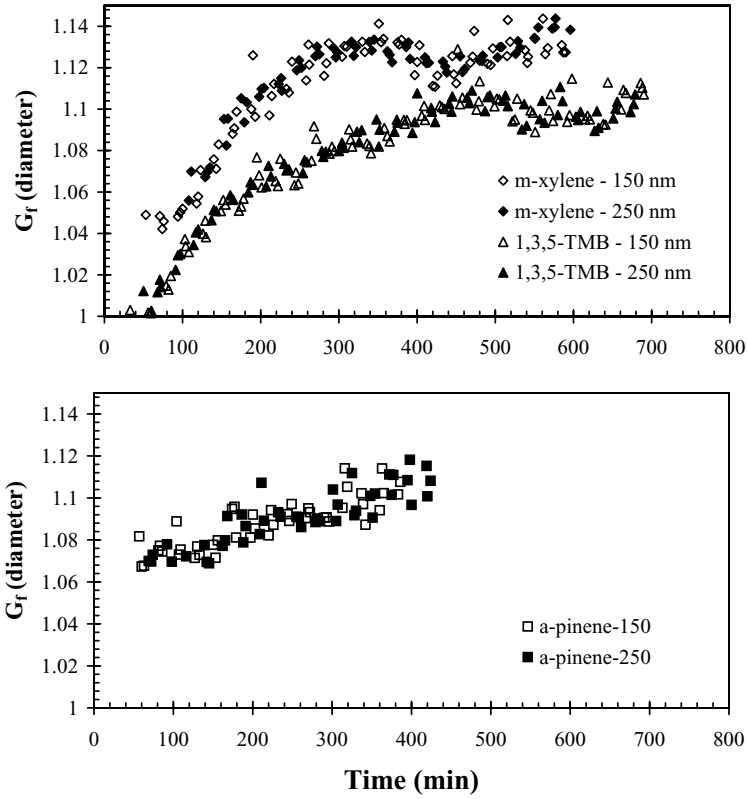

Fig. 1. (a) Hygroscopic growth factors (0–85% RH) for pure *m*-xylene (top) and 1,3,5-TMB (bottom) oxidation products as a function of time. (b) Hygroscopic growth factors (0–85% RH) for pure α-pinene oxidation products as a function of time.

slightly hydrophilic. While the slight upward trend in G_f over the duration of the α-pinene oxidation may indicate some secondary chemistry, G_f never achieves the ultimate level observed for either aromatic system. It appears that the molecular composition of α-pinene oxidation products do not change significantly, as measured by water affinity, over the duration of the oxidation. This near constant value of G_f allows one to estimate the value of G_f based on the volume fractions of organic and inorganic constituents of the aerosol (see Part I) for the α-pinene system; however, for the aromatic systems it is necessary to know the instantaneous value of G_f for the organic portion as a function of time in order to compute the overall value of G_f at any time.

The G_f values obtained for *m*-xylene, 1,3,5-TMB, and α-pinene are consistent with those obtained at 89% RH for the less hygroscopic fraction of ambient urban aerosol. Measurements of the hygroscopic nature of Pasadena, California aerosol (Cocker et al., 2001), carried out over the summer months of 1999, revealed that G_f for the less hygroscopic aerosol mode ranged from 1.03 to 1.17. In the Pasadena study, the lowest G_f values were noted in the early morning, while the highest ones were found in the late afternoon. This increase in G_f may result from increased organic oxidation as the day progresses. The less hygroscopic fraction of urban aerosol was attributed to SOA-coated aerosol. Since, aromatic compounds constitute a significant fraction of gas-phase hydrocarbons in the urban atmosphere, our present results may help explain the measured increase in G_f over the course of a typical day in the Pasadena, California aerosol.

Hygroscopic growth factors were also obtained for *m*-xylene and 1,3,5-TMB at 50% RH over the duration of the photooxidation. At this RH, the measured values of G_f never rose above their initial values ($G_f < 1.01$). The observed G_f values are lower than those for α-pinene at 50% RH ($G_f = 1.04$), even though G_f at 85% RH for the two aromatics exceeds that for α-pinene ozonolysis. The marked increase in G_f for the aromatic compounds as RH increases from 50% to 85% is similar to, but smaller than, that observed for inorganic salts at their RH of deliquescence. Oxidation products of most hydrocarbons contain acids and diacids. It might be expected that an organic acid also deliquesces at

sufficiently high RH, causing the weak acids in the aerosol phase to dissociate (Saxena and Hildemann, 1997). Upon deprotonation, "charge" centers would be created about which water could cluster, drawing even more water into the aerosol and leading to measurable aerosol water uptake. If an α-pinene oxidation product contains a stronger acid than the aromatic oxidation products, the α-pinene RH of deliquescence might be expected to be lower, possibly resulting in water uptake at 50% RH, while *m*-xylene and 1,3,5-TMB oxidation products do not.

When a seed aerosol was present, G_f values were obtained prior to the start of an experiment to verify the state of the seed particles as either deliquesced (aqueous) or effloresced (water-free). G_f for aqueous $(NH_4)_2SO_4$ seed upon humidification from RH 50% to 85% is 1.31, in contrast to the 1.59 G_f for dry $(NH_4)_2SO_4$ seed particles (Nenes et al., 1998).

The liquid water content of the chamber aerosol can be estimated based on the measured G_f. The low G_f measured at 50% RH for particles generated by nucleation under dry conditions implies that very little water is associated with the organic at that humidity. Therefore, it can be assumed that only organic condensation contributes to the increase in the aerosol volume in the chamber; water uptake by the condensed organic is not significant.

4. Effect of relative humidity on SOA formation for *m*-xylene and 1,3,5-TMB photooxidation

The aerosol formation potential of a hydrocarbon is described by its mass-based aerosol yield. The protocols for specific experiments i.e. dry nucleation runs, etc., and the corresponding methods for organic aerosol mass computation are also given in Part I.

Thirty-one and 34 experiments were performed measuring SOA yields from the photooxidation of *m*-xylene and 1,3,5-TMB, respectively. These experiments included ones in which no seed particles were initially present (where aerosol forms by homogeneous nucleation) and with $(NH_4)_2SO_4$ present as either dry inorganic seed particles or an aqueous inorganic seed aerosol. All experiments were performed at temperatures near 293 K. Table 1 summarizes the conditions for each *m*-xylene experiment, including *m*-xylene reacted, NO_x concentrations, aerosol yields, relative humidity, and temperature. Table 2 summarizes the conditions for the 1,3,5-TMB experiments. Fig. 2 shows the yield as a function of the total aerosol mass concentration for all *m*-xylene and 1,3,5-TMB photooxidation experiments. SOA formation was assumed complete when a 1-h plateau in aerosol formation was reached and there was no further measurable decrease in parent hydrocarbon concentration. The data were fit with the two-product absorptive partitioning model, described in Part I (Section 3) assuming that aerosol growth is due solely to the uptake of organic compounds as indicated by the TDMA measurements.

The aerosol yield did not depend upon whether seed particles were, or were not present, on the physical state (aqueous or water-free) of the seed, or on RH. The empirical fits shown in Fig. 2 are the best fits through all the data. Clearly, the water, either vapor or liquid water in the seed aerosol, does not affect the volume of SOA produced in the *m*-xylene and 1,3,5-TMB photooxidation systems investigated.

The agreement between SOA yields for the dry nucleation and the water-free $(NH_4)_2SO_4$ seed experiments confirms that water-free seed simply provides an inert surface upon which condensation can occur and does not affect the gas–particle equilibrium established. These findings are in agreement with Part I of this paper as well as those in Odum et al. (1996, 1997b).

The agreement between the wet nucleation experiments and the water-free experiments demonstrates that increased RH does not increase the volume of aerosol produced from *m*-xylene and 1,3,5-TMB photooxidation. This is expected since gas-phase water is not expected to significantly alter the molecular composition of products. Moreover, TDMA measurements show no change in the volume of *m*-xylene and 1,3,5-TMB photooxidation particles when RH is increased from near zero to 50%. These results agree with those obtained for α-pinene ozonolysis (Part I) after accounting for water uptake of the α-pinene oxidation products as measured by TDMA.

The yield data for aqueous seed at a RH of 50% and for dry seed are also in good agreement, suggesting that the presence of a strong $(NH_4)_2SO_4$ electrolyte solution does not significantly alter the gas–particle equilibrium established for *m*-xylene and 1,3,5-TMB. This result contrasts with that obtained for α-pinene ozonolysis, described in Part I, where gas–particle partitioning was measurably reduced in the presence of a strong, electrolytic aerosol.

It was postulated in Part I that electrolytes in solution may prevent (or at least slow) the aerosol-phase production of hemi-acetals. In systems containing NO, the production of hemi-acetals may be quenched by the NO—peroxyradical reaction leading to minimal hemi-acetal formation in the 1,3,5-TMB and *m*-xylene photooxidation systems. Therefore, the presence of a strong electrolyte would not be expected to have the same effect under conditions where hemi-acetals are not expected to be formed.

It is important to note that hemi-acetals have not been reported in either the α-pinene/O_3 system or the *m*-xylene and 1,3,5-TMB photooxidation systems. However, no analytical techniques have been used to detect the presence of hemi-acetals in these systems.

Table 1
Conditions for *m*-xylene photoxidation experiments

Date	Δ (*m*-xylene) ($\mu g\,m^{-3}$)	$\Delta M_{org+water}$[a] ($\mu g\,m^{-3}$)	NO (ppb)	NO_2 (ppb)	RH (%)	T (°C)	Yield (%)	Seed condition[b]	Amount[c] ($mol\,m^{-3}$)
1/31b	1364.2	175	67.9	75.7	<2	293.3	12.83	Dry	1.5×10^{-7}
1/31a	260.5	10.8	101.1	500	<2	293.3	4.15	Dry	1.4×10^{-7}
3/13a	976.7	98	431.6	218.3	<2	292.8	10.03	Dry	0.3×10^{-7}
3/13b	1744	230.9	241.2	123.5	<2	292.8	13.24	Dry	1.0×10^{-7}
3/23a	632.8	81.6	234.4	101.1	<2	293.2	12.90	Dry	0.9×10^{-7}
4/5a	906.4	113.9	310.1	160.6	<2	293.2	12.57	Dry	1.3×10^{-7}
4/5b	715.8	70	197.3	106.4	<2	293.2	9.78	Dry	2.1×10^{-7}
4/10a	1332.2	184.4	378.9	167.5	<2	293.2	13.84	Dry	0.9×10^{-7}
4/18a	382.7	30.3	68.4	97.2	<2	293.2	7.92	Dry	0.7×10^{-7}
4/27a	1376.9	192.1	431.2	186	<2	293.2	13.95	Dry	2.1×10^{-7}
8/7b	1253.9	168.7	339.4	244.1	<2	293.2	13.45	Dry	2.9×10^{-7}
8/7a	1305.8	163.9	214.4	331.5	<2	293.2	12.55	Dry	2.2×10^{-7}
8/17a	1253.9	159.6	364.3	226.1	<2	293.2	12.73	Dry	1.5×10^{-7}
8/17b	1305.8	160.2	346.7	228.5	<2	293.2	12.27	Dry	1.3×10^{-7}
2/1b	1887.8	265	527.3	267.1	55.4	292.7	14.04	Aqueous	1.2×10^{-7}
2/3b	473.2	28	145.5	169.9	45.3	293.7	5.92	Aqueous	3.2×10^{-7}
2/4a	972.6	102	325.2	179.2	52.1	292.7	10.49	Aqueous	1.9×10^{-7}
2/4b	1244.8	155.9	412.1	207.5	54.7	292.7	12.52	Aqueous	1.3×10^{-7}
3/10a	920.8	71.3	309.1	163.6	49	292.9	7.74	Aqueous	0.4×10^{-7}
3/10b	1249.5	157.3	384.3	196.3	50.5	292.9	12.59	Aqueous	1.1×10^{-7}
3/15a	255.8	13.7	28.3	144.5	48.6	292.9	5.36	Aqueous	0.4×10^{-7}
3/15b	1581.5	221.6	379.9	257.3	49.1	292.9	14.01	Aqueous	2.3×10^{-7}
2/24a	788.8	81	268.1	181.2	<2	294.3	10.27	None	0
2/24b	1136.7	147.8	420.9	225.6	<2	294.3	13.00	None	0
4/3a	424.3	32.6	130.4	67.9	<2	293.2	7.68	None	0
4/3b	1424.8	215	414.6	200.7	<2	293.2	15.09	None	0
3/1a	1263.5	146.5	309.1	198.2	50.6	293.1	11.59	None	0
3/1b	1718.3	230	441.9	214.4	53.6	293.1	13.39	None	0
3/3a	711.8	47.7	200.7	161.1	51.5	292.9	6.70	None	0
3/3b	877	90.6	258.3	181.2	52.3	292.9	10.33	None	0

[a] The increase in aerosol mass caused by the uptake of organic matter and net change in liquid water content. Calculated from Part I, Eqs. (3) and (4).

[b] Seed used was $(NH_4)_2SO_4$ when present.

[c] The quantity of seed listed here was estimated from the observed size distribution and RH as described in Section 6.1 of Part I. It is the amount of aerosol in the chamber 60 min after the lights were turned on, and corresponds to the quantities V_{salt} in Part I, Eq. (3) and $V_{salt+water}$ (when associated with the equilibrium amount of liquid water) in Part I, Eq. (4).

Hemi-acetals are thermally unstable compounds that will decompose in the injection liner of GC–MS or similar analytical instruments. The hemi-acetal argument should not be considered conclusive. Further analytical techniques must be developed to investigate the presence of such oxidation products from the α-pinene/O_3 and 1,3,5-TMB/*m*-xylene photooxidation systems.

Fig. 3 compares the *m*-xylene SOA yield curve obtained here with that obtained in previous studies. The present SOA yields are higher than those in previous experiments, primarily as a result of the lower temperature used for the present experiments (293 K vs 303 K for Kleindienst et al. (1999); 303 K for Izumi and Fukuyama (1990); and approximately 308 K for Odum et al. (1996)). Lower temperatures increase the partitioning coefficient of the products directly ($1/T$ dependence) and indirectly through lower vapor pressures of the semi-volatile oxidation products (exponential dependence of vapor pressure on temperature). Insufficient prior data on the aerosol yield of 1,3,5-TMB at these organic aerosol concentrations precludes comparison of this study with previous ones.

The conclusion that water vapor does not alter the gas–particle partitioning in *m*-xylene and 1,3,5-TMB systems is in agreement with the finding of Edney et al. (2000) that the hygroscopic nature of the photooxidation aerosol products of toluene could be explained by that of the inorganic seed alone.

The primary atmospheric oxidation pathway for the aromatic compounds investigated is through reaction with the hydroxyl (OH) radical. The rate constants for

Table 2
Conditions for 1,3,5-trimethylbenzene experiments

Date	Δ (1,3,5-TMB) ($\mu g\,m^{-3}$)	$\Delta M_{org+water}$[a] ($\mu g\,m^{-3}$)	NO (ppb)	NO_2 (ppb)	RH (%)	T (°C)	Yield (%)	Seed condition[b]	Amount[c] ($mol\,m^{-3}$)
2/11a	1387	61.1	346	300	<2	19.3	4.41	Dry	1.0×10^{-7}
2/11b	1696	78.9	469	297	<2	19.3	4.65	Dry	1.2×10^{-7}
2/19a	1309	60.1	323	415	<2	21.1	4.59	Dry	2.6×10^{-7}
5/11b	2730	195.3	955	447	<2	22.3	7.15	Dry	1.2×10^{-7}
5/17b	3187	249.7	951	453	<2	20.0	7.83	Dry	1.6×10^{-7}
6/21b	3298	257.7	766	352	<2	20.0	7.81	Dry	0.7×10^{-7}
6/26b	3332	257.4	775	392	<2	20.0	7.73	Dry	1.6×10^{-7}
7/5b	3085	244	775	448	<2	20.0	7.91	Dry	0.7×10^{-7}
8/9a	1621	95.7	448	329	<2	20.0	5.91	Dry	3.5×10^{-7}
8/9b	1651	72.9	423	338	<2	20.0	4.41	Dry	3.2×10^{-7}
8/11a	1790	89.2	456	371	<2	20.0	4.98	Dry	1.2×10^{-7}
8/11b	1707	68.8	410	371	<2	20.0	4.03	Dry	1.9×10^{-7}
8/14a	1872	98.9	508	302	<2	20.0	5.28	Dry	1.3×10^{-7}
8/14b	1801	72.8	463	290	<2	20.0	4.04	Dry	2.3×10^{-7}
2/12a	920	29.7	145	255	48.8	19.8	3.23	Aqueous	1.5×10^{-7}
2/12b	1332	62.8	358	263	52.6	19.8	4.71	Aqueous	2.0×10^{-7}
2/14a	1669	56.5	221	428	43.8	20.3	3.39	Aqueous	1.3×10^{-7}
2/14b	1806	111.8	603	361	48.4	20.3	6.19	Aqueous	2.4×10^{-7}
2/15a	1969	99.6	469	367	47.5	20.0	5.06	Aqueous	1.6×10^{-7}
2/15b	1728	94.3	458	363	59.7	20.0	5.46	Aqueous	3.0×10^{-7}
3/17a	975	27.4	289	204	43.7	20.5	2.81	Aqueous	1.8×10^{-7}
3/17b	1350	53.9	383	250	43.4	20.5	3.99	Aqueous	2.9×10^{-7}
3/29a	954	27.1	273	176	46	21.3	2.84	Aqueous	1.2×10^{-7}
3/29b	1353	53.9	399	238	49.6	21.3	3.98	Aqueous	2.1×10^{-7}
6/8a	1920	111.2	537	288	52.7	21.1	5.79	Aqueous	3.5×10^{-7}
6/8b	1780	98.6	372	187	54.3	21.1	5.54	Aqueous	0
2/16a	2584	165	501	454	<2	19.5	6.39	None	0
2/16b	3230	248.7	888	485	<2	19.5	7.70	None	0
2/18a	2659	182.8	748	531	48.4	20.9	6.87	None	0
2/18b	3348	270.9	962	591	48.3	20.9	8.09	None	0
2/21a	1256	50.4	350	207	39.6	20.1	4.01	None	0
2/21b	2048	115.6	564	312	49.5	20.1	5.65	None	0
2/22a	1186	40.5	298	276	48.3	21.2	3.41	None	0
2/22b	1775	82.9	410	310	45	21.2	4.67	None	0

[a] The increase in aerosol mass caused by the uptake of organic matter and net change in liquid water content. Calculated from Part I, Eqs. (3) and (4).

[b] Seed used was $(NH_4)_2SO_4$ when present.

[c] The quantity of seed listed here was estimated from the observed size distribution and RH as described in Section 6.1 of Part I. It is the amount of aerosol in the chamber 60 min after the lights were turned on, and corresponds to the quantities V_{salt} in Part I, Eq. (3) and $V_{salt+water}$ (when associated with the equilibrium amount of liquid water) in Part I, Eq. (4).

OH radical, O_3, and NO_3 radical reactions with *m*-xylene at 298 K are 2.31×10^{-11}, $<3\times10^{-21}$, and $2.6\times10^{-16}\,cm^3\,molecule^{-1}\,s^{-1}$, respectively (Calvert et al., 2000). Similarly, the rate constants for OH radical, O_3, and NO_3 radical reactions with 1,3,5-TMB at 298 K are 5.67×10^{-11}, $<1\times10^{-20}$, and $8.76\times10^{-16}\,cm^3\,molecule^{-1}\,s^{-1}$, respectively (Calvert et al., 2000). Under chamber conditions, *m*-xylene and 1,3,5-TMB react only with the OH radical. As discussed above, the increase in hygroscopicity of the SOA produced over the duration of the photooxidation implies that secondary reactions of the first-generation of oxidation products are occurring. The relative abundances of OH, O_3, and NO_3 may be important in determining the final aerosol yield through further oxidation of products. As varying concentrations of NO_x and hydrocarbon are used, larger experimental scatter in the ultimate SOA yield than for the α-pinene ozonolysis (single oxidant) is expected. The blacklight lamps are unable to reproduce the entire solar spectrum at ground level and therefore some photolytic species may fail to photolyze in the chamber. A thorough comparison of fluorescent blacklights lamps to the solar spectrum and their effect on potential photolytic

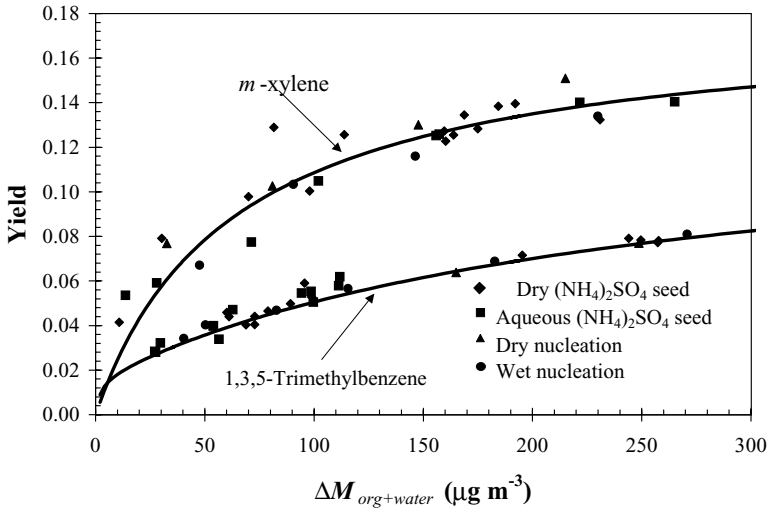

Fig. 2. SOA yield curves for *m*-xylene and 1,3,5-TMB photooxidation experiments. The α_1, α_2, $K_{om,1}$, and $K_{om,2}$ values used to fit *m*-xylene are 0.12, 0.019, 0.06, 0.01, respectively. The α_1, α_2, $K_{om,1}$, and $K_{om,2}$ values used to fit 1,3,5-TMB are 0.016, 0.50, 0.12, 0.004, respectively.

compounds is discussed in detail by Bierbach et al. (1994).

5. Product identification

We attempted to identify and quantify the gas- and aerosol-phase products of *m*-xylene and 1,3,5-TMB under dry conditions. At the onset the goal was to identify enough oxidation products that aerosol yield could be predicted on a molecular basis (Part I). The following sections describe the sampling and identification techniques used, and present the compounds positively identified and quantified. We finish with a discussion of why this methodology failed to identify the vast majority of the products and the need for new techniques to progress in molecular species identification of aromatic oxidation products.

5.1. Sampling techniques

Aerosol-phase products were collected for 1.5 to 6.0 h on the 56 nm stage of a MOUDI ten-stage impactor (MSP corporation, Mineapolis, MN) through a 1.5 m long, 2.2 cm diameter Teflon sampling port positioned in the center of the chamber at a flow rate of 28 LPM. The impactor substrate, a pre-weighed 47 mm punch of aluminum foil, was pre-cleaned by baking at 550°C for 12 h. Gas-phase compounds were collected at a flowrate of 0.35 LPM downstream of the impactors using a series of three impingers pre-filled with 20 ml of de-ionized and organic-free Milli-Q treated water.

5.2. Sample extraction and derivatization

5.2.1. Impactor samples

The impactor substrate was re-weighed after sampling to determine the mass of particulate material collected. A substrate was then loaded into a Soxhlet, spiked with 80 μl of the perdeuterated C_{24} *n*-alkane internal standard solution and extracted for 16–20 h using 100 ml of a 1 : 1 mixture (by volume) of dichloromethane and hexane. For each chamber experiment, a particle-free, blank impactor substrate was also extracted for quality assurance purposes. The sample was derivatized using PFHBA (O-(2,3,4,5,6-pentafluorobenzyl hydroxy amine)) and BSTFA (N,O-bis(trimethylsilyl)-trifluoroacetamide) following the procedure of Yu et al. (1998). The derivatization reaction converts polar compounds into less polar derivatives enabling analysis by GC/MS. Carbonyl groups react with PFBHA to form oxime derivatives and carboxyl and hydroxy groups react with BSTFA to form trimethylsilyl derivatives. Briefly, the derivatization was carried out as follows: after Soxhlet extraction, 2.5 mg of PFBHA was added to the extract and the solution allowed to sit 12–16 h in the dark at room temperature (22–25°C). The extract was then rotary evaporated down to 4 ml, transferred to a 5 ml vial and blown down to 200 μl using a gentle stream of ultra pure N_2. At this point 25 μl of neat BSTFA was added to the extract and the solution was allowed to

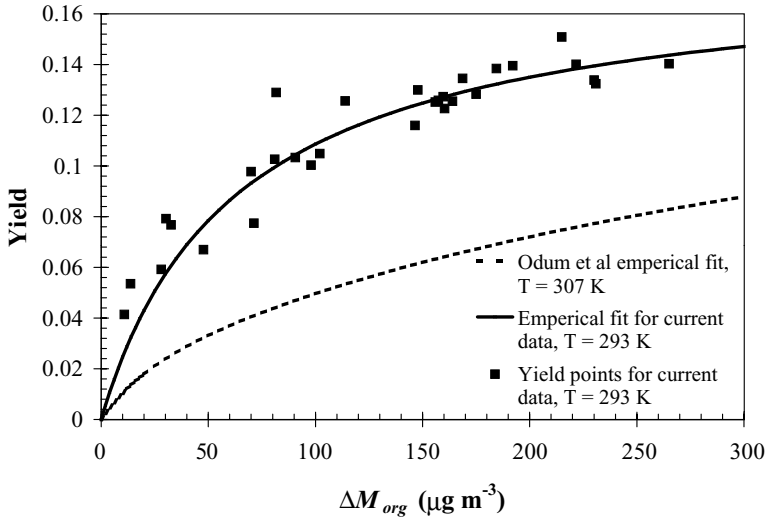

Fig. 3. Comparison of *m*-xylene SOA yield curve in current experiments ($T = 293$ K) to that obtained by Odum et al. (1996) ($T = 307$ K). Izumi and Fukuyama (1990) data points ($T = 303$ K) are in agreement with Odum et al. (1996) yield curve.

reacting for 2 h at 75°C after which time the extract could be analyzed using GC/MS.

5.2.2. Impinger samples

Immediately after sampling, 2.5 mg of PFTBA was added to each impinger. The solution was then allowed to react for 12–16 h in the dark at room temperature. Next, the sample was acidified using six drops of a 36% HCl solution, and the aqueous phase extracted with three 5 ml aliquots of hexane. The sample was evaporated down to 1 ml using a gentle stream of ultra pure N_2, transferred to a 5 ml vial, and further evaporated down to 200 μl. At this point 25 μl of neat BSTFA was added to the extract, and the solution was allowed to react for 2 h at 75°C, after which time the extract was ready for GC/MS analysis.

5.3. GC/MS analysis

Derivatized extracts were analyzed using a Varian Star 3400/Saturn 2000 gas chromatograph/ion trap mass spectrometer operated in electron impact mode. For each experiment 1 μl of an extract was injected in split mode onto the injector. The injector program was as follows: Initial temperature 30°C; after 0.1 min the injector temperature was increased at 60°C/min to 200°C and held for 57 min. Samples were separated using a 25 m, 0.20 mm ID, 0.11 μm film thickness HP-1 capillary GC column (Agilent Technologies, CA). The initial oven temperature was 30°C; after 3 min the oven temperature was increased at a rate of at 3°C/min to 200°C for a total run time of 60 min. On some occasions the run time was extended an additional 10 min and the column temperature set to 300°C. In all experiments the transfer line and ion trap temperature were 180°C and 170°C, respectively. Identified compounds were quantified using authentic standards. Calibration mixtures included all identified compounds and were prepared at five concentrations over the relevant concentration ranges. Compound specific ions and/or mass fragments for the derivatized functional groups were used for quantification. Spiking blank impactor substrates and impingers with standard solutions allowed for recovery experiments of all compounds having authentic standards. The blanks were then extracted and derivatized using the same procedures employed for the actual samples.

5.4. Identification of products in the m-xylene and 1,3,5-TMB photooxidation experiments

Tables 3 and 4 summarize identified products in the *m*-xylene and 1,3,5-TMB photooxidation experiments. Derivatized compounds fragment in a characteristic way; compounds with a carbonyl functional group are identified by the mass m/z 181; those with a carboxyl or hydroxy group, generally produces mass fragments at m/z 73 and 75. In addition the fragments at m/z M-15, M-73, M-89 and M-117, which denote loss of $[CH_3]$, $[Si(CH_3)_3]$, $[OSi(CH_3)]$ and $[C(O)OSi(CH_3)]$ from the derivatized molecule, respectively, are used for identification. Furthermore, the fragment at m/z M-117 is a

Table 3
Carbonyl, alcohol, and carboxylic acid products detected in impactor samples

Peak	RT (min)	Identity	$MW_{derivative}$	MW	*m*-Xylene % of extracted mass	1,3,5-Trimethylbenzene % of extracted mass
	18.44/18.70	Propionaldehyde	253	58	0.64	0.38
PX1[a]	21.10/21.35	C_4 Saturated carbonyl	267	72	Detected	Not detected
PT1[a]	21.63	C_3 Saturated trialcohol or C_2 saturated dihydroxy carboxylicacid	308	92	Not detected	Detected
PX2[a]	22.51/23.09	Possible co-elution of two compounds	NA	NA	Detected	Not detected
PX3[a]	23.28/23.40	Compound with carbonyl and hydroxy groups	NA	NA	Detected	Not detected
	25.75/26.06	Glycolaldehyde	327	60	2.91	6.18
	26.57	Hydroxyacetone	341	74	0.12	0.02
	27.17	Glyoxalic acid	341	74	0.09	0.51
	27.97	Pyruvic acid	355	88	0.14	0.07
PX4[a]	29.34	Compound with carbonyl and carboxylic acid groups	NA	NA	Detected	Not detected
PT2[a]	31.89	Compound with carbonyl and hydroxy groups	NA	NA	Not detected	Detected
	32.66/32.76/33.00	C_5-Oxo-carboxylic acid	383	116	1.05	2.11
	36.77/36.98	Glyoxal	448	58	0.10	0.02
	37.12/37.43/37.73	Methylglyoxal	462	72	2.24	0.72
PX5[a]	38.85	Compound with carbonyl and carboxylic acid groups	NA	NA	Detected	Not detected
PX6[a]	39.81	Compound with carbonyl group	NA	NA	Detected	Not detected
PX7/PT3[a]	41.80	Compound with carbonyl group	504	114	Detected	Detected
			Total percent of extracted mass identified		7.29	10.01

[a] Tentative identification.

characteristic ion only for carboxyl groups; the fragment m/z 147 $[(CH_3)_2Si=OSi(CH_3)]$ is associated with a compound with two carboxyl or hydroxy groups, and m/z 117 $[C(O)OSi(CH_3)]$ is typically observed for compounds having only one carboxyl group. For compounds with carbonyl groups, the mass fragment M-197 $[OCH_2C_6F_5]$ is often observed.

5.5. *m*-Xylene photooxidation

5.5.1. Aerosol phase composition

Fig. 4a shows a chromatogram of the m/z 181, 75 and 73 ions for a filter sample from a *m*-xylene photooxidation experiment. The compounds that are positively identified are indicated, as are those for which only the general structure can be elucidated. A total of 14 peaks are positively identified from the similarity of retention time and mass spectra to authentic standards. Positively identified compounds include: propionaldehyde and glycolaldehyde, whose mass spectra are dominated by a peak at m/z 181; hydroxyacetone, a hydroxyketone, whose mass spectra is also dominated by the m/z 181 ion; and glyoxal, a dicarbonyl, whose mass spectra is dominated by the m/z 147 peak. Three carboxylic acids are observed: glyoxalic acid, pyruvic acid, and a C_5-oxo-carboxylic acid, with observed peaks at m/z 181, 117, 75, and 73, that indicate the presence of carbonyl, carboxyl, and hydroxy functional groups. The C_5-oxo-carboxylic acid and methylglyoxal are quantified using the response factor for 4-oxo-pentanoic acid and glyoxal, respectively. Tentative identifications of 10 peaks are also made on the basis of the compounds' mass spectra. Table 3 summarizes the retention time, identity, and corresponding percentage of the collected aerosol mass for peaks identified using authentic standards. Peaks with only tentative identifications are also included, but not quantified.

5.5.2. Gas-phase composition

Fig. 4b shows a chromatogram combining the m/z 181, 75 and 73 ion peaks for an impinger sample from a *m*-xylene photooxidation experiment. Ten peaks are identified using authentic standards; only the general chemical structure could be elucidated for the other ten-labeled peaks. Several compounds appear in both the gas and particle phases. The compounds identified using

Table 4
Carbonyl, alcohol, and carboxylic acid products detected in impinger samples

Peak	RT (min)	Identity	$MW_{derivative}$	MW	Present in *m*-xylene experiments	Present in 1,3,5-trimethylbenzene experiments
GX1[a]	21.17	C_4 Saturated carbonyl	267	72	Yes	No
GT1[a]	21.63	C_3 Saturated trialcohol or C_2 saturated dihydroxy carboxylic acid	308	92	No	Yes
GX2[a]	22.53	Possible co-elution of two compounds	NA	NA	Yes	No
	25.74/26.05/26.61	Glycolaldehyde	327	60	Yes	Yes
	26.48	Hydroxyacetone	341	74	Yes	Yes
	26.61/27.18	Glyoxalic acid	341	74	Yes	Yes
	27.98	Pyruvic acid	355	88	Yes	Yes
GX3[a]	29.36	Compound with carbonyl and carboxylic acid groups	NA	NA	Yes	No
GX4[a]	31.74/33.05	C_5-Mono-unsaturated-oxo-carboxylic acid	381	114	Yes	No
GT2[a]	31.89	Compound with carbonyl and hydroxy groups			No	Yes
GT3[a]	32.53	Dicarboxylic acid			No	Yes
GT4[a]	32.78	Dicarboxylic acid			No	Yes
	36.76/36.98	Glyoxal	448	58	Yes	No
	37.14/37.76	Methylglyoxal	462	72	Yes	Yes
GX5/GT5[a]	37.42/38.85	Compound with a carbonyl group	NA	NA	Yes	Yes
GT6[a]	40.03	Compound with carbonyl and hydroxy groups	NA	NA	No	Yes
GX6[a]	40.24	Compound with carbonyl and carboxylic acid	NA	NA	Yes	No
GX7/GT7[a]	40.98	Compound with carbonyl and hydroxy groups	NA	NA	Yes	Yes

[a] Tentative identification.

authentic standards are glycolaldehyde, hydroxyacetone, glyoxalic acid, pyruvic acid, glyoxal, and methylglyoxal. The particle phase contains a small quantity of propionaldehyde and a C_5-oxo-carboxylic acid that is not observed in the impinger extracts. This observation may result from the 10-times smaller volume of air sampled through the impingers than is sampled through the impactor. The volume of air collected by the impingers may be insufficient for the detection of propionaldehyde and the C_5-oxo-carboxylic acid. The results are summarized in Table 4. To determine the efficiency of the impingers for gas-phase photooxidation products, a series of three impingers were used. Significant amounts of several compounds were observed in extracts from the final impinger in series. It was impossible to determine whether the three impingers collected 100% of the gas-phase compounds. For this reason, gas-phase concentrations of the identified products are not reported in Table 4.

5.6. 1,3,5-TMB photooxidation experiments

5.6.1. Particle phase composition

Fig. 5a shows a chromatogram of the m/z 181, 75 and 73 ions for a filter sample from a 1,3,5-TMB photooxidation experiment, and indicates the compounds that are positively identified, and those for which only the general structure can be elucidated. A total of 12 peaks were positively identified using authentic standards, and four peaks were tentatively identified on the basis of the mass spectra. Table 3 summarizes the retention time, identity, and corresponding percentage of the collected aerosols' mass for those peaks for which positive identification was possible. Peaks with only tentative identifications are also included but are not quantified. The same products as positively identified for *m*-xylene photooxidation are also positively identified for 1,3,5-TMB photooxidation. Again, the C_5-oxo-carboxylic acid and methyl glyoxal were quantified using the response factor for 4-oxo-pentanoic acid and glyoxal, respectively.

5.6.2. Gas-phase composition

Fig. 5b shows a chromatogram of the m/z 181, 75 and 73 ions from an impinger sample from a 1,3,5-TMB photooxidation experiment. Eight peaks were identified using authentic standards. Only tentative structures could be assigned to eight other peaks. Several compounds were observed in both gas and particle phases.

The compounds identified using authentic standards were glycolaldehyde, hydroxyacetone, glyoxalic acid,

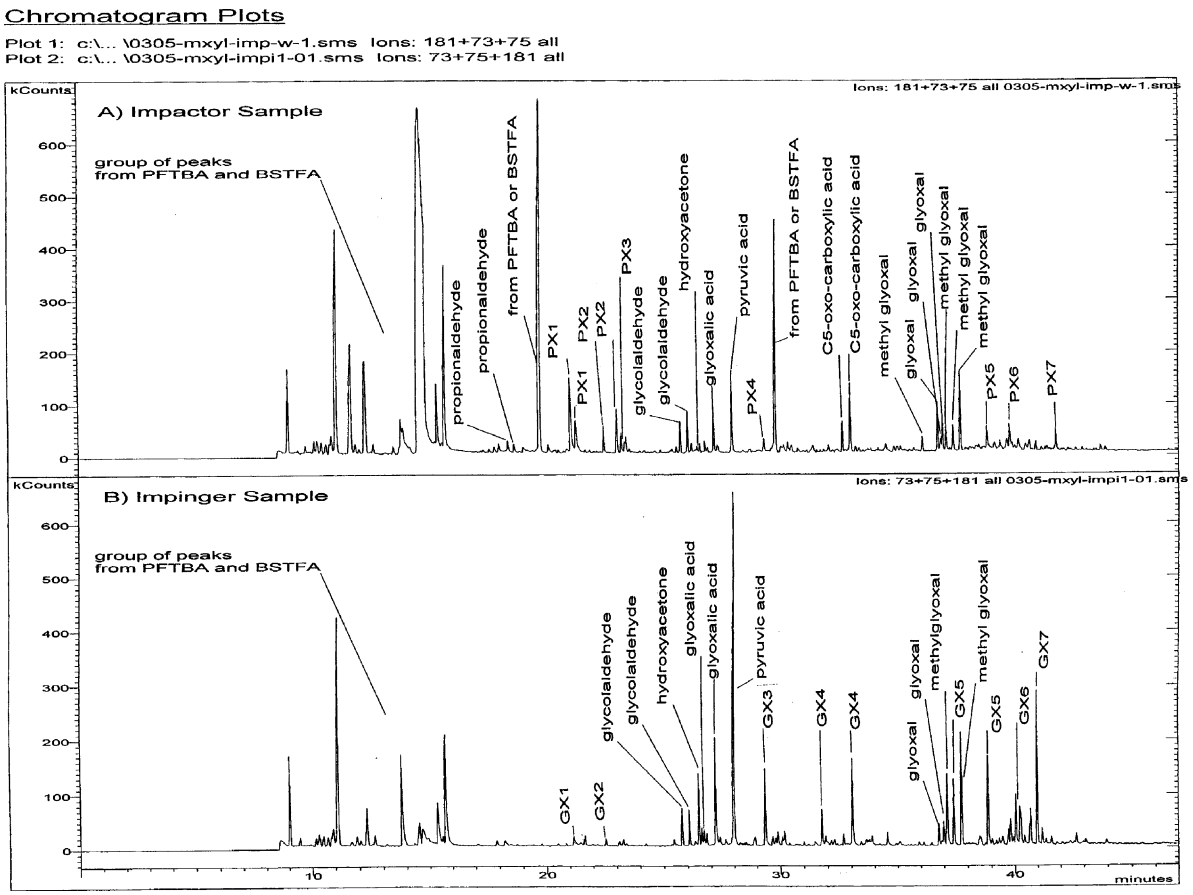

Fig. 4. (a) Chromatogram of impactor sample of *m*-xylene photooxidation showing ions with m/z 181 + 73 + 75 with all carbonyl, carboxylic, and/or hydroxyl compounds identified; (b) chromatogram of impinger sample of *m*-xylene photooxidation showing ions with m/z 181 + 73 + 75 with all carbonyl, carboxylic, and/or hydroxyl compounds identified.

pyruvic acid, and methylglyoxal. Propionaldehyde and glyoxal were found in very small amounts in the particle phase but were not observed in the impinger extracts. Again, the smaller sample volume collected with the impingers may be insufficient to enable detection of propionaldehyde and glyoxal. The results are summarized in Table 4. Concentrations are not given for the same reasons stated in Section 5.5.2.

5.7. Implications of the molecular identification results

Although the major peaks in the chromatogram of the filter samples have been identified, the sum of their masses represents only ~10% of the collected particle mass. It is unlikely that the small, unidentified peaks in the chromatographs constitute the remaining 90% of collected particle mass. Some GC runs were extended to 70 min, reaching column temperatures of 300°C for up to 10 min, but no significant peaks were observed. Furthermore, the compounds that are identified were mostly small, relatively high vapor pressure compounds; it is expected that such compounds would comprise only a small percentage of the particle phase. Since Soxhlet extraction accounted for 96–110% of the collected mass of the impactor samples, it is likely that most of the compounds comprising the SOA do not pass through the GC liner or column. These compounds may have low vapor pressures that limit volatilization from the GC injector, or they may travel very slowly through the column. It is also possible that their polar functional groups do not quantitatively react with the derivatizing reagents; their vapor pressures may not decrease, and/or they may chemisorb on the surface of the GC injector.

Since GC/MS analysis with derivatization appears to be incapable of detecting most of the reaction products, it must be concluded that an alternate analytical technique will be required to make a substantial advance in molecular identification of aromatic aerosol

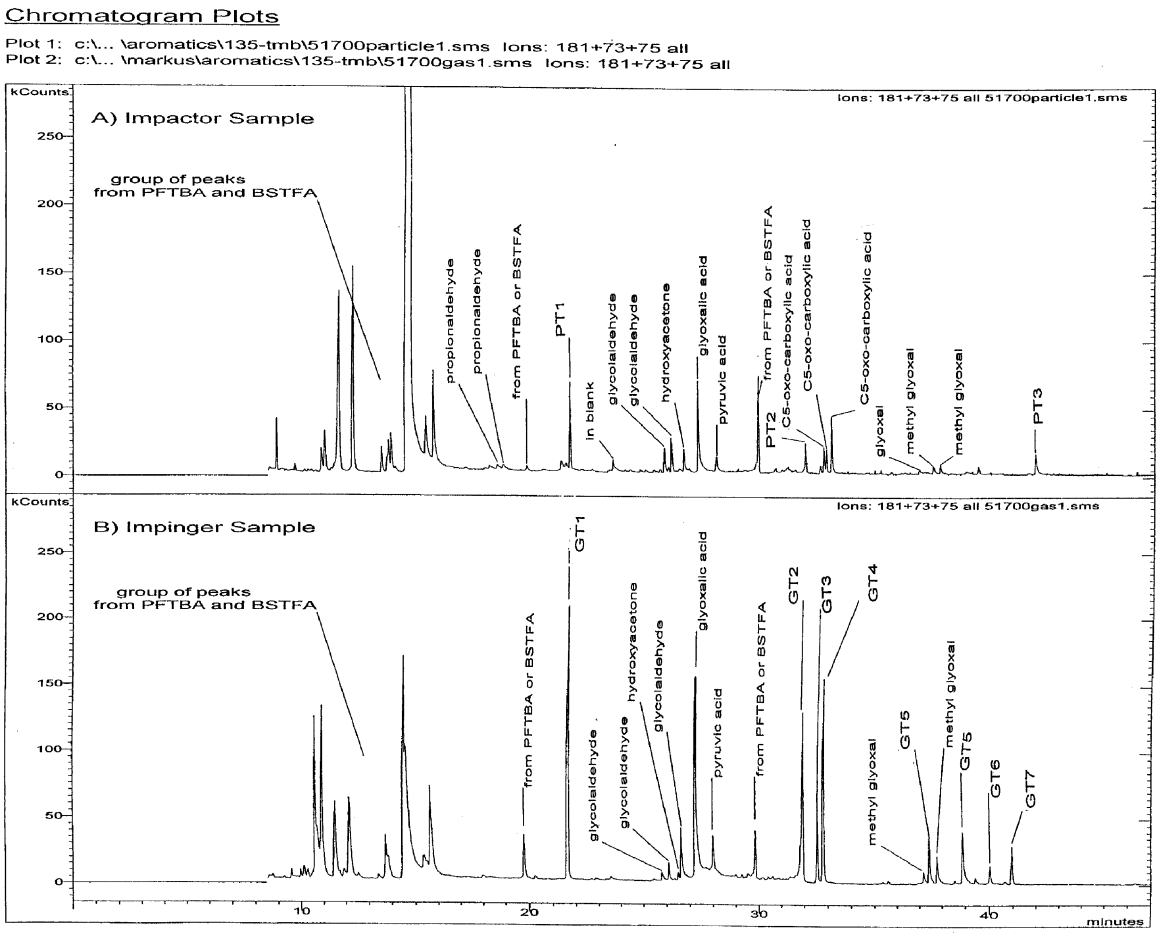

Fig. 5. (a) Chromatogram of impactor sample of 1,3,5-TMB photooxidation showing ions with m/z 181 + 73 + 75 with all carbonyl, carboxylic, and/or hydroxyl compounds identified; (b) chromatogram of impinger sample of 1,3,5-TMB photooxidation showing ions with m/z 181 + 73 + 75 with all carbonyl, carboxylic, and/or hydroxyl compounds identified.

photooxidation products. One such technique to analyze the oxidation products is liquid chromatography–mass spectrometry (LC–MS) which minimizes product losses on the injection liners and eliminates the need to volatilize the products. Furthermore, derivatization is not necessary for transport of the product through the separation column. One major class of expected products is nitrated hydrocarbons for which GC/MS is not ideal (Calvert et al., 2000).

6. Conclusions

The SOA formation potential of *m*-xylene and 1,3,5-TMB is unaffected by the presence of gas-phase and aerosol-phase water or the presence or lack of $(NH_4)_2SO_4$ seed at 50% RH. Hygroscopic growth parameters for *m*-xylene and 1,3,5-TMB oxidation aerosol are found to be negligible at 50% RH and for the SOA produced early in the experiment at 85% RH. However, as the oxidation proceeds, the observed increase in water affinity suggests that the hydrocarbon products undergo further oxidation, by either gas-phase oxidation or aerosol-phase oxidation. A number of the gas- and aerosol-phase photooxidation products were identified, but the majority of the products could not be identified using derivatization/GC–MS techniques. Other techniques will be needed to identify and quantify a significant fraction of the aerosol products of aromatic photooxidation.

Acknowledgements

This work was supported by the US Environmental Protection Agency Center on Airborne Organics, US Environmental Protection Agency Agreement

CR827331-01-0, and the Chevron Corporation. David Cocker was supported in part by a NSF graduate fellowship. Special thanks to K.M. Cocker, N.E. Whitlock, H. Zhuang, and R. Bahreini.

References

Ansari, A.A., Pandis, S.N., 2000. Water absorption by secondary organic aerosol and its effect on inorganic aerosol behavior. Environmental Science and Technology 34, 71–77.

Bierbach, A., Barnes, I., Becker, K.H., Wiesen, E., 1994. Atmospheric chemistry of unsaturated carbonyls—butenedial, 4-oxo-2-pentenal, 3-hexene-2,5-dione, maleicanhydride, 3H-furan-2-one, and 5-methyl-3H-furan-2-one. Environmental Science and Technology 28, 715–729.

Calvert, J.G., Atkinson, R., Becker, K.H., Kamens, R.M., Seinfeld, J.H., Wallington, T.J., Yarwood, G., 2000. Mechanisms of atmospheric oxidation of aromatic hydrocarbons. Final report to Coordinating Research Council, Inc.

Cocker, D.R., Whitlock, N.E., Flagan, R.C., Seinfeld, J.H., 2001. Hygroscopic properties of Pasadena, CA aerosol. Aerosol Science and Technology, in press.

Edney, E.O., Driscoll, D.J., Speer, R.E., Weathers, W.S., Kleindienst, T.E., Li, W., Smith, D.F., 2000. Impact of aerosol liquid water on secondary organic aerosol yields of irradiated toluene/propylene/NO_x/$(NH_4)_2SO_4$/air mixtures. Atmospheric Environment 34, 3907–3919.

Forstner, H.J.L., Flagan, R.C., Seinfeld, J.H., 1997. Secondary organic aerosol from the photooxidation of aromatic hydrocarbons: molecular composition. Environmental Science and Technology 31, 1346–1358.

Izumi, K., Fukuyama, T., 1990. Photochemical aerosol formation from aromatic hydrocarbons in the presence of NO_x. Atmospheric Environment 24A, 1433–1441.

Jang, M., Kamens, R.M., 1998. A thermodynamic approach for modeling partitioning of semi-volatile organic compounds on atmospheric particulate matter: humidity effects. Environmental Science and Technology 32, 1237–1243.

Kleindienst, T.E., Smith, D.F., Li, W., Edney, E.O., Driscoll, D.J., Speer, R.E., Weathers, W.S., 1999. Secondary organic aerosol formation from the oxidation of aromatic hydrocarbons in the presence of dry submicron ammonium sulfate aerosol. Atmospheric Environment 33, 3669–3681.

McMurry, P.H., Stolzenburg, M.R., 1989. On the sensitivity of particle size to relative humidity for Los Angeles aerosols. Atmospheric Environment 23, 497–507.

Nenes, A., Pandis, S.N., Pilinis, C., 1998. Isorropia: a new thermodynamic equilibrium model for multiphase multicomponent inorganic aerosols. Aquatic Geochemistry 4, 123–152.

Odum, J.R., Hoffmann, T., Bowman, F., Collins, D., Flagan, R.C., Seinfeld, J.H., 1996. Gas/particle partitioning and secondary organic aerosol yields. Environmental Science and Technology 30, 2580–2585.

Odum, J.R., Jungkamp, T.P.W., Griffin, R.J., Flagan, R.C., Seinfeld, J.H., 1997a. The atmospheric aerosol-forming potential of whole gasoline vapor. Science 276, 96–99.

Odum, J.R., Jungkamp, T.P.W., Griffin, R.J., Forstner, H.J.L., Flagan, R.C., Seinfeld, J.H., 1997b. Aromatics, reformulated gasoline, and atmospheric organic aerosol formation. Environmental Science and Technology 31, 1890–1897.

Saxena, P., Hildemann, L.M., 1997. Water absorption by organics: survey of laboratory evidence and evaluation of UNIFAC for estimating water activity. Environmental Science and Technology 31, 3318–3324.

Yu, J., Flagan, R.C., Seinfeld, J.H., 1998. Identification of products containing –COOH, –OH, and C=O in atmospheric oxidation of hydrocarbons. Environmental Science and Technology 32, 2357–2370.